Available online at www.sciencedirect.com

ScienceDirect

Ceramics International 40 (2014) 4305–4310

CERAMICS INTERNATIONAL

www.elsevier.com/locate/ceramint

Influence of different surfactants on crystal growth behavior and sinterability of $La_2Ce_2O_7$ solid solution

Yue Wang[a], Chunjie Wang[b,*], Chao Li[a], Yongliang Cheng[c], Feng Chi[b]

[a]College of New Energy, Bohai University, Jinzhou 121013, China
[b]College of Engineering, Bohai University, Jinzhou 121013, China
[c]Laboratory of clean energy chemistry and materials, Lanzhou Institute of Chemical Physics, Chinese Academy of Sciences, Lanzhou 730000, China

Received 25 July 2013; received in revised form 23 August 2013; accepted 23 August 2013
Available online 31 August 2013

Abstract

$La_2Ce_2O_7$ nanocrystals were prepared via hydrothermal method with polyethylene glycol (PEG) and cetyltrimethyl ammonium bromide (CTAB) as surfactants, respectively. X-ray diffraction, thermogravimetric analysis/differential scanning calorimetry, Raman spectroscopy, and Field emission scanning electron microscopy were utilized to characterize the phase structure, thermal decomposition, and morphology of the products. Qualitative analyses indicate that both samples have a cubic fluorite structure. The surfactants have an important effect on the specific surface area, lattice parameter, and average crystallite size of the products. The sample using CATB as surfactant has a higher activation energy of crystal growth than that with PEG. Moreover, the effects of surfactants on the sinterability of compacted body are also discussed.

Keywords: Crystal growth; Surfactant; $La_2Ce_2O_7$; Sinterability; Ceramics

1. Introduction

In recent years, rare earth doped ceria (REC) with a fluorite-type structure has attracted extensive attentions due to its excellent electrical, catalytic, and mechanical properties. The substitution of Ce^{4+} by suitable trivalent cations (such as La^{3+}, Nd^{3+}, and Gd^{3+}) could enhances the chemical stability, increases the ionic conductivity, and suppresses the reducibility of ceria-based materials [1,2].

Among various REC, $La_2Ce_2O_7$ has received many research attentions owing to its unique properties as well as potentially wide applications. In consideration of the above factors, considerable efforts have been paid to the investigation of $La_2Ce_2O_7$. Cao et al. studied the thermophysical properties of $La_2Ce_2O_7$ [3]. Benjaram et al. reported the structural characteristics and catalytic performance of $La_2Ce_2O_7$ [4]. Andrievskaya et al. devoted their work to the phase relation of La_2O_3–CeO_2 system at 1100–1500 °C [5]. However, most above studies were focused on the bulk materials, the difference of crystal growth and sintering–resistance properties of nano-sized $Ln_2Ce_2O_7$ materials, as far as we know, have not yet been reported. It is well known that nanomaterials exhibit superior properties (such as mechanical, electrical, and thermal properties) compared to the conventional coarse-grained counterparts. On the other hand, during the heat treatment, two competitive processes namely crystallization and sintering are included [6]. In general, crystallization makes densification more difficult, so it is necessary to investigate the crystal growth behavior. The absence of systematic and reliable information will lead to contradictory statements about the stability of the system. To improve the physicochemical properties of materials, it is quite essential to make insight into the characteristics at the nanolevel.

Generally, different types of surfactants have different effects on the physicochemical properties of the products. The structure, crystal growth, and sinterability are significant properties for ceramics materials. The appropriate surfactant should have beneficial effect on such respects. Unfortunately, up to date, the systematic comparison of the effects of surfactants on the physicochemical properties of $La_2Ce_2O_7$ has not been reported.

*Corresponding author. Tel.: +86 416 3400573.
E-mail address: cjwang@foxmail.com (C. Wang).

0272-8842/$ - see front matter © 2013 Elsevier Ltd and Techna Group S.r.l. All rights reserved.
http://dx.doi.org/10.1016/j.ceramint.2013.08.096

In this paper, we report our recent work regarding the fabrication of $La_2Ce_2O_7$ via hydrothermal process with PEG and CTAB as surfactants. The effects of the kinds of surfactants on the structure, crystal growth, and sinterability of the produced $La_2Ce_2O_7$ and compacted body were investigated. The main purpose of this study is to explore more favorable surfactant for ceramics materials, which can enhance the understanding and broaden the database of thermodynamic properties of REC.

2. Experimental

In this paper, the nanocrystalline $La_2Ce_2O_7$ were synthesized via the conventional hydrothermal method. La_2O_3 (99.9%, Guangdong Chenghai Sanxing Chemicals Ltd.) and $Ce(NO_3)_3 \cdot 6H_2O$ (99.9%, Shanghai Chemicals Ltd.) were used as starting materials. Firstly, appropriate amounts of La_2O_3 were dissolved in concentrated nitric acid and then mixed with a stoichiometric $Ce(NO_3)_3 \cdot 6H_2O$ aqueous solution to give a final molar concentration of 0.1 M. After homogenization, a certain amount of PEG (2 wt%, Shanghai Chemicals Ltd.) as surfactant was added into this solution. The pH value of the solution was adjusted to 7 by adding sodium hydroxide solution (2 M). The nanocrystalline powders were then obtained by hydrothermal treatment for the suspension in a Teflon autoclave at 180 °C for 24 h. The precipitates were filtered and washed with distilled water and ethanol for several times, and then dried at 70 °C for 12 h. The same procedure was followed for the preparation of $La_2Ce_2O_7$ nanocrystalline powders by using CTAB as surfactant. In this paper, both two samples were designated as LC-PEG and LC-CTAB in the text, respectively.

For crystal growth investigations, some powders were calcined at different temperatures. A typical regime involved a heating rate of 5 °C min^{-1} to the selected temperatures and then cooling down at 5 °C min^{-1} after soaking for 5 h.

The crystalline phases of $Ln_2Ce_2O_7$ nanocrystalline powders calcined at different temperatures were identified by powder X-ray diffraction (XRD, Bruker D8 Focus powder X-ray diffractometer) using Cu Kα radiation ($\lambda = 1.5406$ Å) with a scanning rate of 5° min^{-1}. The operation voltage and current were maintained at 40 kV and 40 mA, respectively. The apparent mean crystallite size of powders (D) was determined by Scherrer's equation [7]:

$$D = \lambda \frac{K}{\beta \cos \theta} \quad (1)$$

where λ is the wavelength of the X-ray radiation, θ is the diffraction angle, K is a constant (0.89) and β is the corrected full-width half maximum (FWHM). For the instrument correction, the Gaussian–Gaussian relationship was used [7,8]:

$$\beta^2 = B^2 - b^2 \quad (2)$$

where FWHM of the sample is represented by B, and b is for the standard width of reference silicon sample.

The thermal behavior studies of the dried powders were carried out from room temperature up to 1200 °C using thermogravimetric analysis and differential scanning calorimeter (TG/DSC) with a heating rate of 10 K min^{-1} in a Netzsch STA 449C Jupiter apparatus. FT–Raman spectra were recorded on a Thermo Nicolet 960 instrument with an excitation wavelength of 1064 nm.

In order to further investigate the sintering behavior of $Ln_2Ce_2O_7$ powders, disk-shaped samples with a diameter of 11 mm and a thickness of 3 mm were prepared by cold isostatic pressing (CIP) at 220 MPa. Subsequently, the sample was sintered at 1500 °C for 5 h. Microstructure of the sintered body was observed via scanning electron microscope after polishing.

3. Results and discussion

The thermal behaviors of both samples were investigated by TG/DSC as shown in Fig. 1. The simultaneous TG/DSC can give us some qualitative information about the thermal behaviors of both samples. In the case of TG curves, for LC-PEG, a

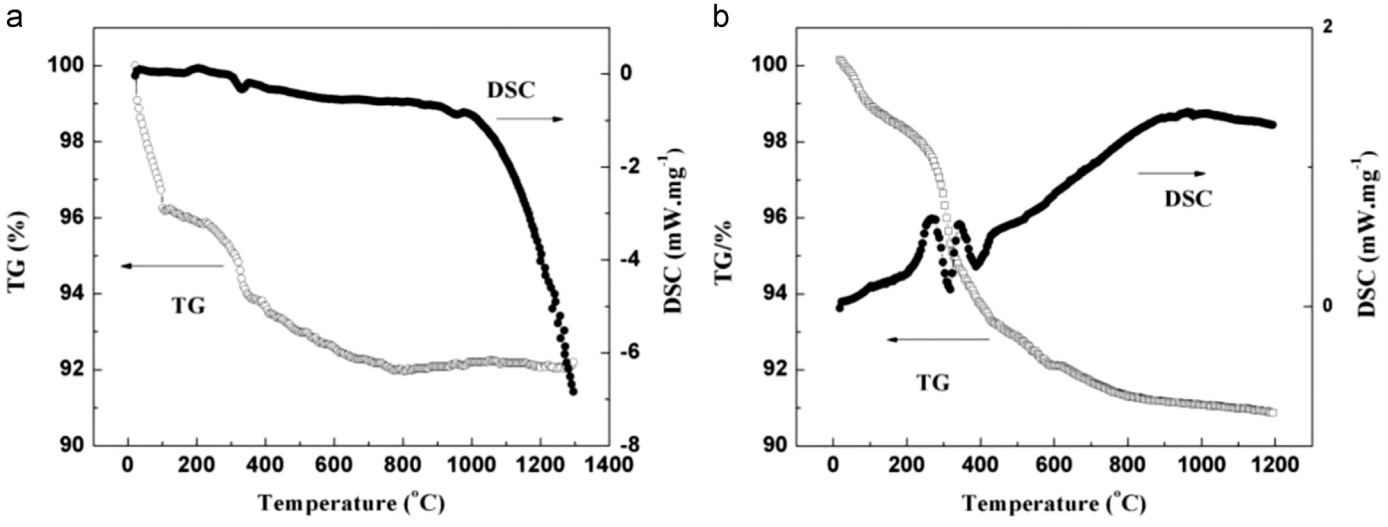

Fig. 1. The TG/DSC curves of the as-prepared products: (a) LC-PEG and (2) LC-CTAB.

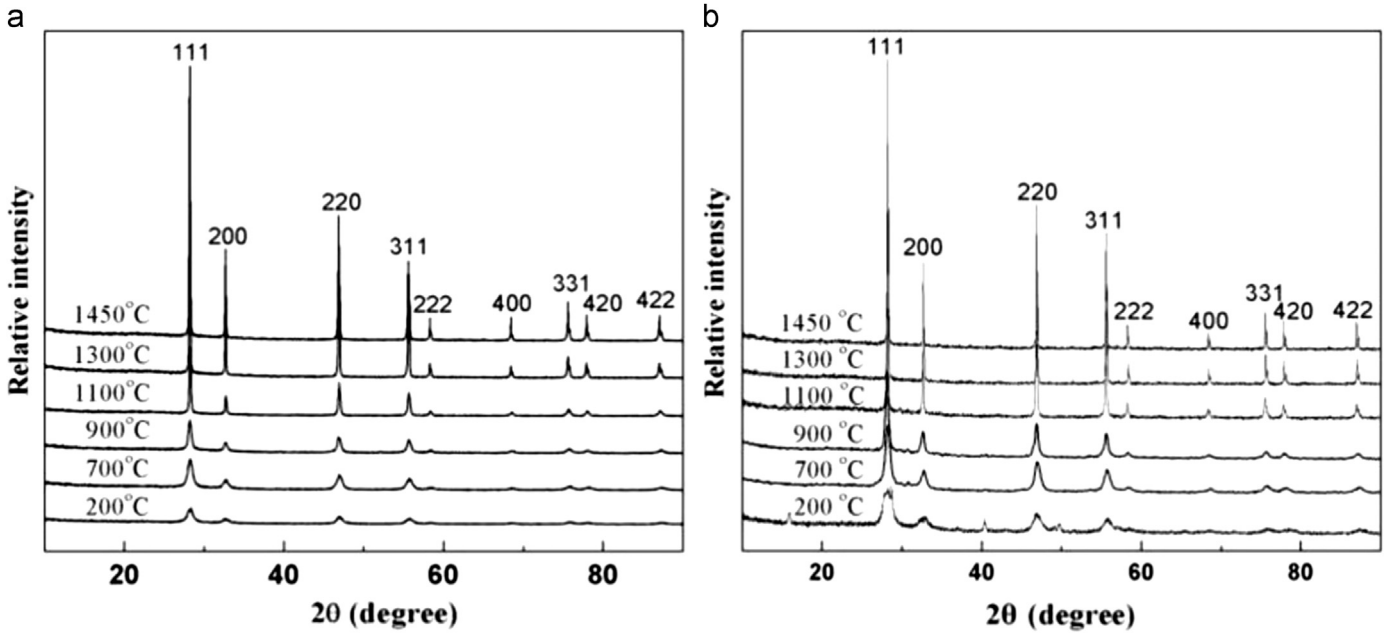

Fig. 2. XRD patterns of $La_2Ce_2O_7$ nanocrystals with different surfactants calcined at various temperatures: (a) LC-PEG and (b) LC-CTAB.

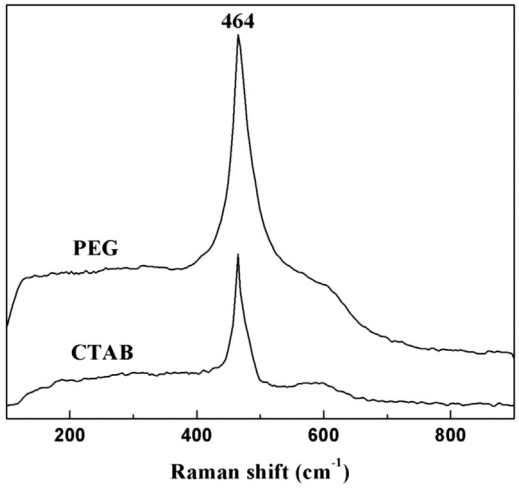

Fig. 3. Raman spectra of LC-PEG and LC-CTAB calcined at 1100 °C.

significant mass loss about 7.98% can be observed. Nevertheless, the overall weight loss of LC-CTAB is approximately 9.14%. Furthermore, for the TG curve of LC-PEG, the weight loss could hardly be observed at temperature above 800 °C implying a complete decomposition of organic substances, and this temperature is lower than that of LC-CTAB (about 900 °C). For both samples, the mass loss mainly derived from the evaporation of physically absorbed water and decomposition of nitrates and organic substances [9]. The difference amount of the decomposition products lead to the variation of mass loss.

In the case of DSC curves, two exothermic peaks can be observed from 300 to 420 °C in both samples, which may be attributed to the elimination of residual organic substances formed during synthesis or subsequent ethanol-washing processes [9]. For LC-CTAB, the intensity of peaks is higher than that of LC-PEG. The exothermic peak near 950 °C is resulted from the grain coarsening, including the bulk crystallization process [10].

Based on the TG/DSC results, both samples were calcined at different temperatures and further analyzed by XRD at room temperature, as shown in Fig. 2. Detailed analysis indicates that both sample's XRD patterns match well with the standard cubic fluorite phase of CeO_2, and no evidence of pyrochlore phase (*Fd3m*) could be found. For LC-PEG, the diffraction peaks of all samples located at 28.2°, 32.6°, 46.8°, and 55.6° can be well indexed to the (111), (200), (220), and (311) planes of a cubic fluorite structure, respectively. The absence of diffraction peaks around 36.9 and 44.5 are always considered as the characteristic of fluorite structure distinguished from pyrochlore structure [11]. The diffraction peaks become sharper and narrower with the increase of calcination temperature, implying that the crystal size increases and the crystallinity of $La_2Ce_2O_7$ becomes better. In addition, no characteristic peaks corresponding to the individual oxides (La_2O_3 etc.) can be observed in all curves within the scope of XRD diffraction, and this disparate feature can be attributed to which indicates the formation of $La_2Ce_2O_7$ solid solution. Similarly, the LC-CTAB has the same case compared to LC-PEG (Fig. 2 (b)). There is no more different between these two series curves.

Both samples calcined at 1100 °C were further investigated by Raman spectroscopy in the frequency range of 100–900 cm^{-1}, as represented in Fig. 3. Careful investigation of the spectra revealed a detailed structure of fluorite type. Clearly, in the case of LC-PEG, the main peak at 465 cm^{-1} of two samples corresponds to the F_{2g} Raman band from the space group of *Fm3m* of a cubic fluorite structure. Furthermore, as shown in the Fig. 3, the intensity of the band

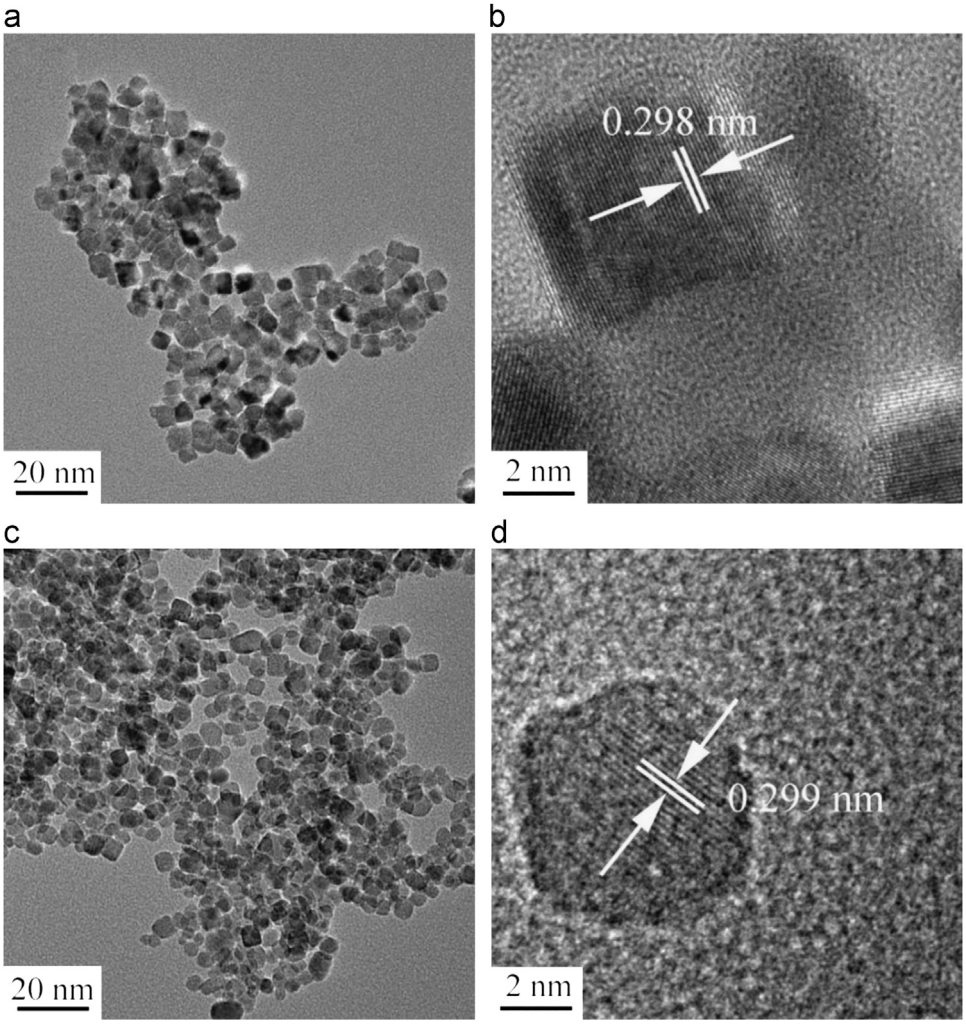

Fig. 4. TEM and HRTEM of as-obtained $La_2Ce_2O_7$ nanocrystals: (a, b) LC-PEG and (c, d) LC-CTAB.

at 465 cm^{-1} is higher for LC-PEG as compared to that of LC-CTAB. In addition, a small shoulder at 600 cm^{-1} assigned as a longitudinal optical mode arises due to the relaxation of symmetry rules [12]. In the present case, it can be reasonably considered that the incorporation of La^{3+} into a CeO_2 matrix results in the formation of oxygen vacancies, giving the formation of defect-induced band in the spectrum. Thus, Raman scattering further confirmed the possibility of the incorporation of La^{3+} in CeO_2 matrix as previously indicated by the XRD analysis mentioned above.

The morphology, particle size, and structure of the synthesized materials were illustrated by TEM and HRTEM, respectively. Typical TEM images of both samples are compared in Fig. 4(a) and (c), respectively. By contrast, LC-PEG shows a cubic shape with the particle size ranging from 10 to 12 nm, and LC-CTAB has an aspheric morphology (the particle size between 8 and 10 nm). The average particle sizes of both samples obtained from TEM patterns are consistent with that calculated from Scherrer's equation. Moreover, HRTEM was employed to obtain the internal structure of the produced nanocrystallites. The atom arrangements in crystals can be observed in Fig. 4(b) and (d), and the interplanar distance in the nano-sized crystals can be estimated. The determined distance was obtained from the averaged value of ten planar distances selected randomly. As shown in Fig. 4(b) and (d), the magnified HRTEM images clearly reveal the lattice fringes with a *d-spacing* of 0.298 nm (Fig. 4(b)) and 0.299 nm (Fig. 4(d)) correspond well with the (111) lattice plane of cubic fluorite $La_2Ce_2O_7$.

In addition, the crystallite size, specific surface area, and lattice parameter are also investigated, as shown in Table 1. LC-PEG has a specific surface area of 195.59 $m^2\ g^{-1}$, which is higher than that of LC-CTAB (187.53 $m^2\ g^{-1}$). The lattice parameter calculated from the XRD patterns for LC-PEG is 0.5432 nm, which is lower than that of LC-CTAB (0.5498 nm). Furthermore, the average crystallite size is obtained by Scherrer's equation as mentioned in above. For LC-PEG, the average crystallite size for LC-PEG is 9.27 nm, while that of LC-CTAB is 11.36 nm, which consistent with the result form the TEM observation. It is reasonable to expect that the different selective adsorption processes and the interactions between the surfactant and inorganic precursor molecules during the nucleation process could affect the structure, surface area, crystallite size and organization of nanocrystals.

Table 1
The crystallite size, specific surface area, lattice parameter, volume shrinkage, and relative density of LC-PEG and LC-CTAB.

Samples	Crystallite size at 180 °C (nm)	Specific surface area ($m^2\ g^{-1}$)	Lattice parameter (nm)	Volume shrinkage (%)	Relative density (%)
LC-PEG	9.27	195.59	0.5432	11.3	62.1
LC-CTAB	11.36	187.53	0.5498	19.5	75.2

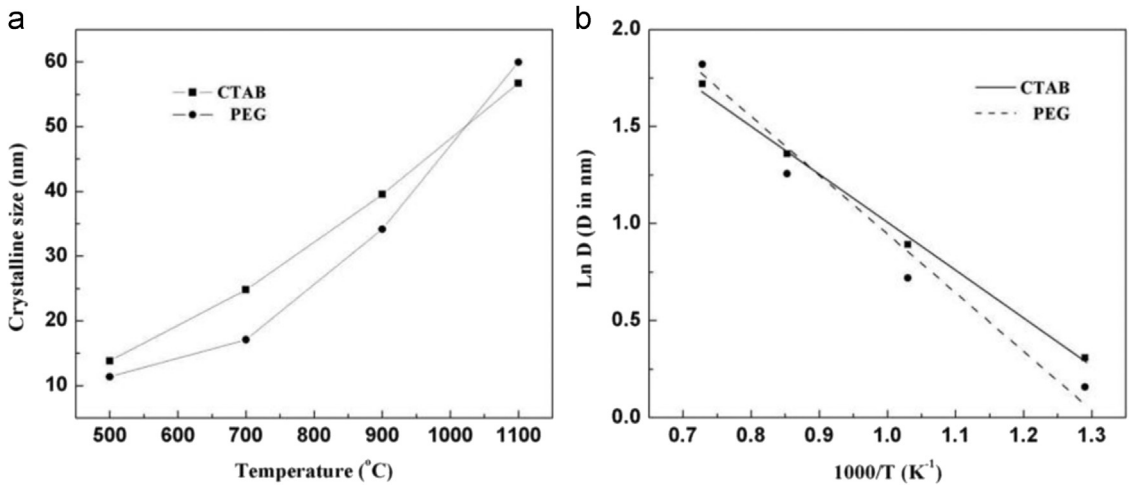

Fig. 5. Effects of calcination temperature on the nanocrystallite sizes of LC-PEG and LC-CTAB (a) and plots of ln (D) against 1000/T (b).

However, the related mechanism is more complicated needs to be further investigated.

Some powders were also calcined at different temperatures to further understand the influence of surfactants on the crystal growth behavior, and the activation energy of crystal growth (Q) was also estimated. Fig. 5(a) shows the relationship between the calcination temperature and the average size of sample prepared by different surfactants. The logarithms of average crystallite size versus the reciprocal of the calcination temperature are plotted in Fig. 5(b) by linear fitting, assuming that the crystal growth is a thermally activated process. According to Eq. (3):

$$D_t = D_0 \times e^{(-Q/RT)} \tag{3}$$

where D_0 and D_t are the initial and final average nanocrystallite size (nm) calculated by Scherrer's equation, R denotes the ideal gas constant (kJ K^{-1} mol^{-1}), T is the calcination temperature (K) [13]. Therefore, the activation energy of crystal growth can be obtained by calculating the slope of ln (D) versus 1000/T (Fig. 4(b)). The obtained activation energies for LC-PEG and LC-CTAB are 15.27 ± 0.03 and 16.33 ± 0.02 kJ mol^{-1}, respectively. This fact indicates that the addition of CTAB can increase the activation energy of the crystal growth. It is well known that the activation energy is closely related to crystal growth during the heat treatment process. Also, there is a close association between crystal growth and sinterability for ceramics materials. The higher activation energy is, the lower the growth rate will be, which has a beneficial effect on the sinterability for ceramics materials. Unfortunately, the mechanism of surfactants effects on the activation energy of crystal growth is scarce in the literatures. As we known, the synthetic route has an important role on crystal growth [14]. The chemical factors (such as adsorbed atoms) could completely alter the original surface energy and affect the critical crystallite size [15,16]. On the other hand, the presence of vacancy defects must have a significant influence on the crystal growth. Deeper researches on the mechanism are in progress, which will be published elsewhere.

In order to investigate the effect of surfactants on the sinterability, both sample were compacted at 220 MPa and further sintered at 1500 °C for 5 h. The theoretical density was calculated from lattice parameter measurements by XRD. The sintered densities were typically obtained by weighing the samples and determining their volume by the Archimedes method, expressed as a percentage of the theoretical density, as shown in Table 1. After sintering at 1500 °C for 5 h, the volume shrinkage of LC-PEG is about 11.3%, while that of LC-CTAB is 19.5%. On the other hand, the relative densities of LC-PEG and LC-CTAB are 62.1 and 75.2%, respectively.

The SEM micrographs from the thermally etched surfaces of LC-PEG and LC-CTAB sintered compacts are compared in Fig. 6. Both samples show completely different morphologies after processed at high temperature. As shown in Fig. 6(a), LC-PEG has a porous networking microstructure. Such porous body exhibits numerous channels and pores on its surface, and these channels and pores seem to be connected to each other. The abnormal growth of grains could also be found. These interconnected open channels and pores prohibit the further densification of LC-PEG. Such an open structure may have a potential application in oxygen sensors, catalyst supports, etc.

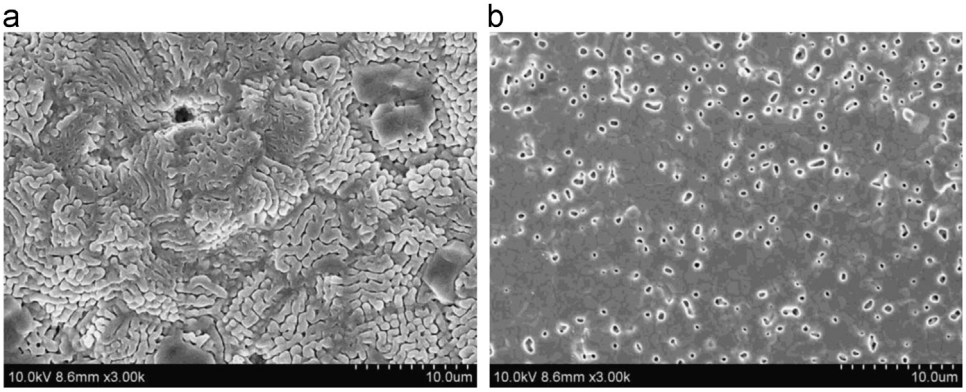

Fig. 6. SEM images of LC-PEG (a) and LC-CTAB (b) bodies sintered at 1500 °C for 5 h.

However, in the case of LC-CTAB, the grain size is about 1.36 μm with some pores (0.97 μm) can be observed, as shown in Fig. 6(b). A certain amount of pores has an important effect on reducing the average thermal expansion coefficient of the materials [17]. Also, the interfaces between particles were very clean and no other interphases or unreacted oxides existed in the interfaces, and no abnormal growth of grains could be found. By contrast, the sinterability of LC-CTAB is better than that of LC-PEG. By taking all the above results into account, it can be concluded that CTAB as surfactant has a significant effect on improving the sinterability for $La_2Ce_2O_7$ compared to the sample with PEG as surfactant.

4. Conclusions

$La_2Ce_2O_7$ nanocrystallines were synthesized via hydrothermal method with PEG and CTAB as surfactants. Both samples are fluorite structures. The surfactants have a significant influence on the morphology, specific surface area, lattice parameter, average crystallite size, and activation energy of crystal growth. The sintered body of LC-PEG has an open structure which has a potential application in oxygen sensors and catalyst carriers. The sample with CTAB shows a better sinterability than that using PEG as surfactant.

Acknowledgment

This work was financially supported by the National Natural Science Foundation of China under Grant no. 11247284.

References

[1] Y. Wang, H. Guo, S.K. Gong, Thermal shock resistance and mechanical properties of $La_2Ce_2O_7$ thermal barrier coatings with segmented structure, Ceramics International 35 (2009) 2639–2644.
[2] J.S. Bae, W.K. Choo, C.H. Lee, The crystal structure of ionic conductor $La_xCe_{1-x}O_{2-x/2}$, Journal of the European Ceramic Society 24 (2004) 1291–1294.
[3] X.Q. Cao, R. Vassen, W. Fischer, F. Tietz, W. Jungen, D. Stover, Lanthanum–cerium oxide as a thermal barrier-coating material for high-temperature applications, Advanced Materials 15 (2003) 1438–1442.
[4] Benjaram M. Reddy, L. Katta, G. Thrimurthulu, Novel nanocrystalline $Ce_{1-x}La_xO_{2-y}$ ($x=0.2$) solid solutions: structural characteristics and catalytic performance, Chemistry of Materials 22 (2010) 467–475.
[5] E.R. Andrievskaya, O.A. Kornienko, A.V. Sameljuk, A. Sayir, Phase relation studies in the CeO_2–La_2O_3 system at 1100–1500 °C, Journal of the European Ceramic Society 31 (2011) 1277–1283.
[6] H. Dai, X. Zhong, X. Cao, Neodymium-cerium oxide as new thermal barrier coating material, Surface and Coatings Technology 201 (2006) 2527–2533.
[7] H. Jin, N. Wang, L. Xu, S. Hou, Synthesis and conductivity of cerium oxide nanoparticles, Materials Letters 64 (2012) 1254–1256.
[8] S.A. Hassanzadeh-Tabrizi, M. Mazaheri, M. Aminzare, S.K. Sadrnezhaad, Reverse precipitation synthesis and characterization of CeO_2 nanopowder, Journal of Alloys and Compounds 491 (2010) 499–502.
[9] A.A. Bukaemskiy, D. Barrier, G. Modolo, Physical properties of 8 mol% ceria doped yttria stabilised zirconia powder and ceramic and their behavior during annealing and sintering, Journal of the European Ceramic Society 26 (2006) 1507–1515.
[10] P. Zhang, A. Navrotsky, B. Gou, I. Kennedy, A.N. Clark, Energetics of cubic and monoclinic yttrium oxide polymorphs: phase transitions, surface enthalpies, and stability at the nanoscale, Journal of Physical Chemistry C 112 (2008) 932–938.
[11] C. Wang, W. Huang, Y. Wang, Y. Cheng, X. Cao, Synthesis of monodispersed $La_2Ce_2O_7$ nanocrystals via hydrothermal method: A study of crystal growth and sintering behavior, International Journal of Refractory Metals and Hard Materials 31 (2012) 242–246.
[12] Z. Xu, S. He, L. He, X. Cao, Novel thermal barrier coatings based on $La_2(Zr_{0.7}Ce_{0.3})_2O_7$/8YSZ double-ceramic-layer systems deposited by electron beam physical vapor diposition, Journal of Alloys and Compounds 509 (2011) 4273–4283.
[13] C. Wang, Y. Wang, Y. Cheng, W. Huang, B. Zou, X. Cao, Effects of surfactants on the structure and crystal growth behavior of $Sm_2Zr_2O_7$ nanocrystalline, Powder Technology 225 (2012) 130–135.
[14] S.G. Chen, Y.S. Yin, D.P. Wang, Experimental and theoretical investigation on the correlation between aqueous precursors structure and crystalline phases of zirconia, Journal of Molecular Structure 690 (2004) 181–187.
[15] D. Moldovan, V. Yamakov, D. Wolf, S.R. Phillpot, Scaling behavior of grain-rotation-induced grain growth, Physical Review Letters 89 (2002) 206101–206104.
[16] W. Huang, J. Yang, X. Meng, Y. Cheng, C. Wang, B. Zou, Z. Khan, Z. Wang, X. Cao, Effect of the organic additions on crystal growth behavior of ZrO_2 nanocrystals prepared via sol–gel process, Chemical Engineering Journal 168 (2010) 1360–1368.
[17] C. Wang, Y. Wang, Y. Cheng, W. Huang, X. Cao, Preparation and thermophysical properties of nano-sized $Re_2Zr_2O_7$ (Re=La, Nd, Sm and Gd) ceramic with pyrochlore structure, Journal of Materials Science 47 (2012) 4392–4399.